A Study of the Ionized Gas in the Galactic Plane using Radio Recombination Lines near 327 MHz

D. Anish Roshi
National Centre for Radio Astrophysics,
Tata Institute of Fundamental Research (TIFR),
Post Bag 3, Ganeshkhind, Pune 411 007.

Thesis supervisor: Prof. V. K. Kapahi

Ph.D. Thesis, University of Pune.
July, 1999.

Dedicated with affection
to my late father
and
to my mother

Contents

Acknowledgments

I am deeply indebted to Prof. K. R. Anantharamaiah, my unofficial thesis advisor. He first introduced me to the fascinating problems and questions related to Radio Recombination Lines and suggested that I build a spectrometer to study the same. His subsequent active collaboration in the project made the study a reality. It was a pleasurable learning experience working with him. I owe my training in research methodology to him. In spite of his several other commitments he always found the time to help and guide me in my work. Thank you Anantha.

My adviser (late) Prof. V. K. Kapahi was extremely helpful to me in several matters related to this thesis. He allowed me a lot of freedom in my work which I greatly appreciated – his sudden death was a tremendous loss to me.

I am particularly indebted to Prof. Gopalkrishna who agreed without hesitation to take over the responsibility of being my adviser and completing all thesis formalities on the demise of Prof. Kapahi. In this regard, I wish also to thank Prof. A.W. Joshi, Head of the Dept. of Physics, Pune University, who took personal interest in helping me sort out several formalities at the University.

Prof. A. Pramesh Rao was extremely supportive of this work. He took it upon himself to sort out many practical difficulties that arose while I was working on this project. Also he was ever willing to give of his time to discuss the technical aspects of the project. I am deeply grateful to him.

I would like to specially thank Ravi Subrahmanyan who first acquainted me to the working of the autocorrelation spectrometer that he built. I learnt a lot also from the many discussions I had with him. My thanks are also due to A. J. Selvanayagam for suggesting crucial modifications to a part of the analog design. P. K. Manoharan, A. J. Selvanayagam and Niruj Mohan (JAP, RRI, Bangalore) were very helpful during the measurement of the dynamic range of the ORT receiver system. Many thanks to A. A. Deshpande, RRI, Bangalore, who suggested useful methods to improve the performance of the multi-line spectrometer.

In the initial stages of this project, Prof. T. Velusamy's interest in the project and support in all matters were a great help. Dr. V. Balasubramanian took much interest in the project and helped in speeding up the completion of PCB designs. My thanks to both of them.

I am grateful to all those who have helped me in building the multi-line spectrometer – P. V. Mahesh for first helping me build the receiver and later helping me with the observations; Dominic, Leslie and Martin for making the mechanical boxes and racks for the system; C. Ravindran, CRL, Ooty, for doing the back-plane wire wrapping; S. Illango for building the 16 bit add-on card. Others I must mention specially are S. Ramesh, R. Chandrasekaran, C. Satheesh, R. Venkatasubramani, K. Athmanathan, A. M. Poonuttu, Muralidaran, C. Balakrishnan, D. Muthukrishnan, K. G. Aravindakrishnan and D. Nandagopal.

I thank V. Raghunathan, D. Ravikumar, A. Bilal, S. Srinivasan and V. Venkatasubramani for helping me in observing using the Ooty Radio Telescope. I am grateful to all the other staff members at the Radio Astronomy Centre, Ooty, for providing excellent support during the building of the multi-line spectrometer and during the observations

.

I am also grateful to Raman Research Institute, Bangalore, for partially funding the project and allowing me use of their computer and library facilities. The staff at the library and computer centers of RRI were always supportive and ready to help.

I am grateful to Jayaram Chengalur for the discussions I had with him. The discussions were extremely useful and helped in clarifying several details related to this work.

I thank M. Vivekanand for the many discussions and encouragement especially during his stay at RAC, Ooty. My thanks are due to Nimisha G. K. and Y. Gupta for reading the proof of the thesis and suggesting improvements in the presentation. I also thank Prof. G. Swarup for his encouragement and interest in this observational project.

I wish to acknowledge Prof. F. J. Lockman for providing his data on H II regions and Prof. T. Handa and Prof. W. Reich for providing their continuum maps.

Thanks to the members of my family for patiently awaiting the completion of this work. My wife has supported and encouraged me. Many thanks to her.

Declaration

The work presented in the thesis "A Study of the Ionized Gas in the Galactic Plane using Radio Recombination Lines near 327 MHz" by D. Anish Roshi is original and has not formed the basis for award of any other degree or diploma of any other University or Institution.

D. Anish Roshi

Prof. Gopalkrishna
(Dean, NCRA)

Abstract

In this thesis we present an observational study of an extended low-density ionized component in the galactic disk. The tool used for the investigation is radio recombination lines (RRLs) near 327 MHz. The observations were made using the Ooty Radio Telescope (ORT). A new multi-line spectrometer, capable of observing eight RRL transitions simultaneously with a spectral resolution of $\sim$ 1 km s^{-1} , was specially built for these observations. The thesis describes details of the equipment used for the observations, data reduction procedures, the observations and results. Detailed interpretation of the data in terms of the distribution of the low-density ionized gas in the galactic plane and its physical properties forms a major part of the thesis. A possible origin of the low-density gas is also discussed at the end of the thesis.

Radio recombination lines are spectral lines emitted when free electrons recombine to very high quantum states of an ion and then cascade down the energy levels. The phenomenon occurs in both fully and partially ionized regions. Observations of RRLs are useful for studying the properties of different types of ionized gas in the Galaxy. The galactic plane contains several types of ionized gas such as the warm ionized medium (WIM), the hot ionized medium (HIM) and H II regions. The WIM and HIM are part of the general interstellar medium (ISM) with large volume filling factors ($f \sim 0.2 - 0.5$). The WIM has an average electron density $< n_e > \sim 0.25$ cm^{-3} with a typical electron temperature $T_e \sim 10^4$ K and the HIM has $T_e \sim 10^6$ K and $< n_e > \sim 0.003$ cm^{-3} (McKee & Ostriker 1977, Kulkarni & Heiles 1988). H II regions are formed around young and "hot" stars and typically have $T_e \sim 10^4$ K and a range of densities and sizes. At one extreme are the ultracompact H II regions which have density $n_e > 10^5$ cm^{-3} and size < 0.1 pc. At the other extreme are the evolved diffuse H II regions with $n_e \sim 1 - 100$ cm^{-3} with sizes of a few tens of parsecs. In addition to the very low-density distributed ionized components of the ISM (WIM & HIM) and the relatively high density H II regions (which occupy only a small volume of the Galaxy), there is observational evidence for a low-density extended ionized component in the inner Galaxy. This component has been referred to as "extended low-density" (ELD) ionized gas by Mezger (1978) and as "extended low-density warm ionized medium" (ELDWIM) by Petuchowski & Bennett (1993), Heiles (1994) and Heiles, Reach & Koo (1996).

From the theory of RRLs, it can be shown that the low frequency lines ($\leq$ 1.5 GHz) originate from low-density ionized gas and thus form an ideal tool to study the extended low-density gas. Observationally, this low-density ionized gas in the inner Galaxy was identified through the detection of low frequency RRLs at several positions along the galactic plane which are free of discrete continuum sources (Gottesman & Gordon 1970, Gordon & Cato 1972). Subsequently, this low-density component has been systematically observed in radio recombination lines near 1.4 GHz by Hart & Pedlar (1976b), Lockman (1976; 1980), Cersosimo (1990) and Heiles et al. (1996). Recombination lines from this gas was also observed by Anantharamaiah (1985a; 1985b) near 325 MHz. This thesis concerns new extensive observations of this low-density ionized component in radio recombination lines at frequencies near 327 MHz using the ORT.

The detection of low-frequency RRLs from almost all observed positions in the galactic longitude range 0° to 40° has led to different suggestions for the origin of the low density gas. For example, Shaver (1976) has suggested that they are large ($\sim$ 100 pc in size) low-density H II regions whereas Mezger (1978) has referred to this gas as an "extended low-density" (ELD) component, which is ionized by field OB stars that are not located in radio H II regions. On the other hand, Anantharamaiah (1986) has argued that this low-density gas is simply the outer envelopes of the normal (usually higher density) H II regions. A similar suggestion has been made by Hart and Pedlar (1976a) based on their study of W3, W4 and W5 H II region complexes. The possible association of the low-density ionized gas with the normal H II regions was also suggested by Lockman (1980). Based on the ubiquity of RRL emission in the inner

Galaxy as seen in their recent observations near 1.4 GHz, Heiles et al. (1996) have associated the lines with the ELDWIM. They picture the ELDWIM as a version of the local WIM in the galactic interior with $< n_e^2 >$ large enough to produce observable RRLs near 1.4 GHz.

There are other observational evidences for the presence of an extended low-density ionized component in the galactic disk. These include (i) the *COBE* (Cosmic Microwave Background Explorer) observations of widespread far-infrared fine structure transitions of C II (λ = 158 μm) and N II (λ = 205 μm) in the galactic plane, (ii) "turnovers" seen in the continuum spectrum of galactic supernova remnants and extragalactic continuum sources at frequencies $<$ 100 MHz, (iii) absorption of galactic nonthermal background emission at frequencies $<$ 100 MHz and (iv) occurrence of enhanced scattering of radio waves in the inner Galaxy. The results from these observations are discussed briefly in the thesis.

A large scale survey of RRLs at a low frequency is extremely time consuming. This is because the lines are very weak (line to continuum temperature ratio is $\sim 10^{-3}$) requiring long integrations ($>$ 15 hours per position) to detect them. To reduce the actual observing time, we built a new multi-line spectrometer which is capable of observing eight RRLs simultaneously with a spectral resolution of $\sim$ 1.0 km s^{-1} . We observed two sets of four adjacent recombination line transitions with this spectrometer. At the observing frequency the nearby RRL transitions carry the same physical information. Hence the eight spectra are eventually averaged to improve the signal to noise ratio and reduce the observing time by a factor of eight. A detailed description of the multi-line spectrometer is presented in the thesis.

The key to understand the extended low-density ionized gas in the inner Galaxy is to determine its physical properties such as density, temperature and sizes of the regions and to determine the distribution of the gas in the galactic plane. To estimate the physical properties of the line emitting gas, it is essential to use multi-frequency observations. A complete survey of the galactic plane is required for understanding the distribution of the ionized gas in the disk. With these objectives in mind, we have made a survey of RRLs near 327 MHz in the galactic plane using the ORT. The RRL transitions observed are the H270α, H271α, H272α and H273α. The observing strategy was the following. Observations were made in the two longitude ranges of the galactic plane that can be observed with the ORT. These ranges are l = 332^o to 0^o to 89^o, referred to as the inner Galaxy, and l = 172° to 252°, the outer Galaxy. The inner Galaxy was observed with two different angular resolutions – (a) 2° × 2° (low resolution mode) and (b) 2° × 6′(high resolution mode). Higher resolution (2° × 6′) is obtained by using all the 22 'modules' of the ORT, which together form a telescope of size 530 m × 30 m, and the lower resolution (2° × 2°) is obtained by using only a single 'module' of the ORT, which effectively is a telescope of size 24 m × 30 m. In the low resolution mode, we made an unbiased contiguous sampling of the galactic plane in the inner Galaxy and also observed 14 positions (b = 0°) in the outer Galaxy. To study the latitude extent of the line emission, we observed over ± 4° along galactic latitude at two specific longitudes (l = 0° & 13°.9). In the high resolution mode, we sampled a selected set of 2° and 6° wide fields in the inner Galaxy. About 300 spectra were obtained in all these observations, which cover a total sky area of $\sim$ 345 square degree. These observations form the largest body, yet obtained, of low frequency recombination line data. The observations, results and the interpretation of the hydrogen line emission in the galactic plane form the main theme of the thesis.

In the low resolution survey, hydrogen RRLs were detected at almost all positions in the inner Galaxy. In the outer Galaxy, lines were detected towards only three positions. The observations as a function of the galactic latitude detected lines up to $b \sim \pm 3°$. The line emission is well correlated (correlation coefficient = 0.88) with the largely nonthermal continuum emission in the same direction indicating the dominance of stimulated emission. The median width of the observed line is 31 km s^{-1} which is larger than the median line widths observed from normal H II regions. These data are used in this thesis to derive the distribution of the low-density ionized gas in the galactic disk and to obtain constraints on

the physical properties of the ionized gas. The results are compared with other observations in the galactic plane.

The longitude-velocity (lv) diagram obtained from the low resolution survey data shows some concentration of hydrogen line emission in the spiral arms at longitudes $l < 50°$. The distribution of RRL emission near 327 MHz as a function of galactocentric distance shows a sharp peak near 4 kpc with more than 70 % of the emission originating between 2.5 kpc and 6 kpc. The lv diagram and the radial distribution obtained from the present data shows good similarity with that of RRL emission near 1.4 GHz, "intense" ^{12}CO emission and to some extent with the RRLs observed near 3 cm from normal H II region. These distributions are distinctly different from that of Hα emission and H I emission from the galactic disk. The difference in the distribution between RRL and Hα is mainly due to obscuration by dust of the Hα emission and difference in sensitivity of recombination lines in optical and radio bands. Based on the similarity in the distribution of RRL emission at 327 MHz, ^{12}CO emission at 3 mm and RRL emission at 3 cm from normal H II regions, we conclude that the diffuse RRL emission in the galactic disk is associated with star forming regions. We also conclude that most of the line emission near 1.4 GHz originates from the ionized gas which is responsible for the RRL emission near 327 MHz.

Combining RRL observations near 1.4 GHz with our data, we derived constraints on the physical properties of the gas producing the line emission. A brief discussion of the theory of RRLs and the details of the modeling used for deriving the physical properties are presented in the thesis. The measured line strengths at 1.4 GHz and 327 MHz place a good constraint on the density of the ionized gas. The derived densities are in the range 1 - 10 cm^{-3} . Using the measured continuum near 10 GHz and 2.7 GHz, the upper limit on the RRL intensity near 75 MHz and the dispersion measure ($\int n_e dl$) obtained from the electron density model by Taylor & Cordes (1993), we obtain upper limits on the temperature and the physical size of the ionized region in different directions. The upper limits obtained for the temperature are typically 10000 K and that for the pathlengths are typically 600 pc. In a few positions, the upper limits on the electron temperature, as obtained from the width of the line, are less than 4800 K. By assuming a temperature of 7000 K for the ionized cloud, we estimated the sizes of the line emitting region. The estimated sizes are in the the range 20 - 200 pc.

Using the derived physical properties of the clouds that produce RRL emission near 327 MHz, we estimated the expected C II 158 μm and N II 205 μm line emission from these low-density ionized clouds. We found that most of the N II emission and a considerable fraction of the C II emission observed by the *COBE* satellite could originate in the ionized gas responsible for RRL emission. We also computed the expected free-free absorption of the galactic nonthermal emission near 34.5 MHz due to the presence of these ionized clouds. We again found that a considerable fraction, if not all, of the absorption of the background radiation at low frequencies < 100 MHz towards the galactic plane could be due to the low density ionized gas which is responsible for the observed RRL emission near 327 MHz.

The higher resolution ($2° \times 6'$) observations were used to study the clumpiness of the low-density ionized gas in the galactic plane. The fields that were observed using the full ORT are positions where lines were detected in the low resolution survey made using a single module of the ORT. In the higher resolution observations, the hydrogen lines were detected at almost all positions within all the five selected fields with $l < 35°$. However, at many positions the parameters of the detected line are found to vary considerably on angular scales of $6'$. Beyond $l = 35°$, although lines were not detected at many individual positions, the integrated spectrum obtained by averaging the spectra at different positions within a $2° \times 2°$ area shows the presence of line emission. A detailed study of the data from one of the fields, G45.5+0.0, shows that the line emission extends to regions beyond the $2° \times 6'$beam area although the lines were detected only towards three individual positions within the field. Averaging subsets of spectra spanning different angular regions within the field G45.5+0.0

resulted in lines with different parameters indicating that the line emitting region is quite clumpy. We estimate that the sizes of the clumps can be as large as one degree or more. There exists some evidence for the association of these clumps with known H II regions within this field.

Finally, we consider in this thesis the origin of the low-density ionized gas in the galactic disk. The pathlengths obtained for the ionized gas from the RRL observations are in the range 20 – 200 pc implying that the filling factor of this medium is only 1% or less. This low filling factor clearly indicates that the low-density gas is not a pervasive medium. Analysis of the RRL emission in the disk shows that the global distribution of the ionized gas responsible for the line emission is similar to that of star forming regions. This similarity suggests that the line emitting zones may be associated with normal H II regions. H II regions with large low-density outer components are expected from models of star formation (Zuckerman 1973). Recent study of the luminosity function of OB associations in the Galaxy also indicates that radio H II regions have envelopes that absorb $\sim 2/3$ of the ionizing photons from the H II regions (McKee & Williams 1997). Thus, in our opinion, the low frequency RRLs originate from extended low-density components associated with normal H II regions. The low-density gas does not form a pervasive medium as might be suggested by the term 'extended low-density warm ionized medium (ELDWIM)' which has been used in the literature to describe this component (Mezger 1978, Petuchowski & Bennett 1993, Heiles 1994, Heiles, Reach & Koo 1996).

Chapter 1

Introduction

Our Galaxy consists of various forms of matter including neutral and ionized gases. Ionized gases occur in different forms and they constitute a large component of the medium between the stars (known as the ISM – the Interstellar Medium). This thesis concerns ionized gases with densities in the range 0.5 and 10 cm^{-3} . The tool used here to study these ionized gases are observations of radio recombination lines (RRLs) at frequencies near 327 MHz. Observations were obtained using the Ooty Radio Telescope (ORT) which operates at this frequency. In this chapter, we present a brief overview of the different types of ionized gases present in the Galaxy and an introduction to the use of RRLs in their study. The chapter concludes with a preview of the work presented in this thesis.

1.1 Ionized components of the Galactic ISM

At visible wavelengths, the conspicuous and numerous objects seen in the sky are stars. However, the tenuous matter contained in the region between the stars (the ISM) is not visible to the naked eye. The total mass of matter in the ISM is a few percent of that of the stars in the Galaxy. The ISM is both a cradle and a crematorium for stars. Massive stars take material from the ISM during their birth, process the material to produce heavier elements and replenish the ISM during their death. Thus the ISM plays a vital role in the evolution of the Galaxy. Matter in the ISM is in various forms – ionized, neutral and molecular. Understanding the physical properties of these components, such as their temperature, density, size, their distribution and role in the evolution of the Galaxy are active research areas in Astrophysics – both observationally and theoretically. We focus here on the different types of ionized regions in the ISM.

Hot Ionized Medium

Observations of soft X-ray background and O VI absorption lines (cf. review by Kulkarni & Heiles, 1988) indicate the presence of a large amount of hot, low-density gas in the disk of our Galaxy. This is known as the hot ionized medium (HIM) or the coronal gas. The temperature of the HIM is $\sim 10^6$ K and average electron density $< n_e > \sim 0.003$ cm^{-3} (McKee & Ostriker 1977). The average volume filling factor of this component in the galactic disk may be ~ 50 % (Ferriere 1998). All the other components of the ISM are believed to be embedded in the HIM. The HIM is believed to be generated by supernovae and stellar winds from hot stars.

Warm Ionized Medium

The presence of a widely distributed warm ionized medium with $< T_e > \sim 8000$ K is evident from diffuse Hα emission (Reynolds 1983, 1995). This medium is believed to be responsible for the observed dispersion of pulsar signals. The mean electron density estimated from pulsar observations is ~ 0.03 cm^{-3} . The volume filling factor of this component is ~ 20 %. The WIM is ionized by ultraviolet (UV) photons ($\lambda \leq 912$ Å) from hot ($T > 30{,}000$ K) O and B stars.

H II regions

There are other forms of ionized gas in the ISM which have relatively small volume filling factors. These are hot ionized clouds surrounding bright stars, commonly known as emission nebulae, because their spectra exhibit emission lines. They are classified further into H II regions, planetary nebulae and supernova remnants. H II regions are of relevance to this study. Their electron densities range between $\sim 1 - 10^5$ cm^{-3} and they have a relatively narrow range of temperatures ($T_e \sim 3000 - 10000$ K). The sizes of these regions range from a fraction of a parsec to tens of parsecs. At one extreme are the ultra-compact H II regions with $n_e > 10^4$ cm^{-3} and sizes < 0.1 pc, which are formed around very young hot stars (Wood & Churchwell 1989), still embedded in their parent molecular clouds. At the other extreme are the diffuse evolved H II regions of low density.

Extended Low-density Ionized Gas

Somewhere in between the very low-density, distributed ionized components of the ISM, namely the WIM and the HIM, and the relatively high density H II regions (which occupy only a small volume of the Galaxy), there appears to be an extended low-density ionized component in the inner Galaxy ($|l| < 60°$). This component has been referred to as "extended low-density" (ELD) ionized gas by Mezger (1978), "H II –envelopes" by Lockman (1980) and Anantharamaiah (1986) and as "extended low-density warm ionized medium" (ELDWIM) by Petuchowski & Bennett (1993), Heiles (1994) and Heiles, Reach & Koo (1996b). The main theme of the thesis is a study of these low-density regions.

Partially Ionized Regions and Ionized Gas in other components of the ISM

All the components of the ISM that are discussed above are fully ionized and are relatively hot. Cool ($T_e \sim 100$ K) regions on the outer boundaries of the H II regions, with a fractional ionization of $\sim 10^{-2} - 10^{-3}$, called Partially Ionized Medium (PIM), are formed by ionization of hydrogen due to soft X-rays from the central stars or shock fronts, and ionization of carbon by far-UV photons of energy > 11.3 eV which are leaking out of the Strömgren sphere. An example of an observation of radio spectral lines from such a PIM is shown in Fig. 1.1. The far-UV photons from the central stars of H II regions can travel long distances through the ISM to regions not only adjacent to H II regions but also the neutral ISM and the surfaces of molecular clouds producing PIMs where carbon is ionized. The latter have been referred to as photo-dissociation regions (PDRs) because the far-UV photons dissociate the molecules in the H II region-molecular cloud interface. Thus in the PDRs and the neutral component of the ISM, the carbon atoms are fully ionized although hydrogen ionization fraction is small.

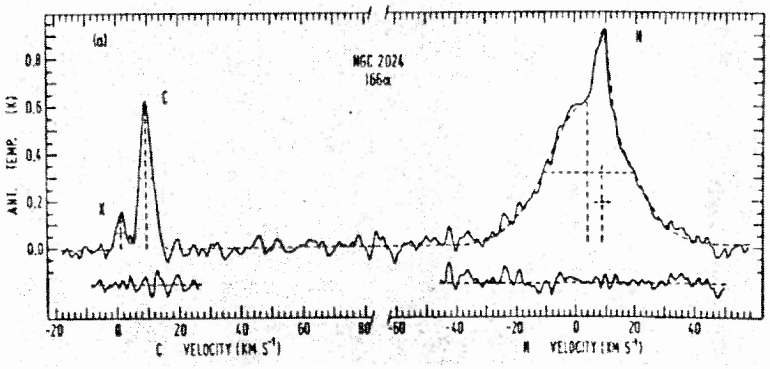

Figure 1.1: The 166α spectra of NGC2024. The Gaussian fits are indicated by the dashed lines. Note that the hydrogen line is fitted with a broad and narrow Gaussian whose centers and half power widths are also marked. The narrow component originates from the partially ionized medium adjacent to the H II region producing the broad component. The residuals after fitting the Gaussians are shown below each profile (from Pankonin et al. 1977).

1.2 Radio Recombination Lines

Recombination lines are spectral lines emitted when free electrons in an ionized gas recombine to very high quantum states of an ion and then cascade down through the energy levels. The spectral lines due to transitions from principal quantum numbers above 25 to the nearby energy levels fall in the radio frequency regime (ν <300 GHz; photon energies less than 1.2×10^{-3} eV). These lines are analogous to the $H\alpha$ lines ($\Delta n = 1$ transition of Balmer series; $\lambda = 6562.8$ Å) seen at optical wavelengths. Radio recombination lines (RRLs) are some of the weakest spectral lines observed in astronomy. The possibility of detecting such lines from ionized gas in astrophysical situations was first predicted by Kardashev (1959). The prediction was first confirmed by Dravskikh and Dravskikh (1964) and Sorochenko and Borodzich (1964) who detected recombination lines in the direction of M17 and the Orion nebula near 5 GHz. Subsequent observations have detected such lines from several galactic objects and also from other galaxies. RRLs have been observed over a wide range of frequencies from 14 MHz to 300 GHz. RRLs of hydrogen, helium, carbon and sulphur are detected from different astrophysical objects. RRLs of different elements can be identified from the respective shift in the centroid frequency of the observed line, which is due to the difference in reduced mass.

Recombination lines are normally detected from H II regions. The gas in an H II region is ionized by ultraviolet photons from the hot star. At sufficiently great distances from the central star, an equilibrium is established between ionization and recombination of free electrons. The recombined electrons cascade down the energy states to produce a series of spectral lines. Observation of these lines can be used to constrain the physical properties of the gas emitting the lines. The physical parameters of interest are the electron temperature, the electron density and the size of the line emitting

region. The Doppler shift of the centroid frequency of the spectral line with respect to its rest frequency yields the radial velocity of the source. The location of the line emitting region in the Galaxy can be determined from the measured radial velocity using a model for galactic rotation. RRLs as a tool in astrophysics have been used to trace the spiral arm pattern of the Galaxy (Georgelin and Georgelin 1976), for measuring the variation of abundance of heavy elements as a function of galactocentric distance, determining the temperature of the H II region at different locations in the Galaxy (see for e.g. Shaver et al. 1983) and determining the helium to hydrogen abundance ratio in the Galaxy (see review by Mezger 1980, Shaver et al. 1983, Roelfsema & Goss, 1992).

1.3 Low-density Ionized Gas in the Galactic disk

There are several observational evidences for the presence of a low-density ionized component in the inner Galaxy ($|l| < 60°$). Here we briefly review these observations.

1.3.1 Evidence from Low-frequency Recombination Lines

From the theory of RRLs it can be shown that lines at low frequencies (< few GHz) do not originate in normal high-density H II regions due to the effects of continuum opacity, pressure broadening and beam dilution (Shaver 1975). Observations of low frequency RRLs are therefore sensitive to relatively low density ($0.5 < n_e < 50$ cm^{-3}), large angular size (tens of arcminutes) ionized regions. Low frequency RRL observations, made in the early 70's, have detected lines at several positions along the galactic plane in the inner Galaxy which are free of discrete continuum sources (Gottesman & Gordon 1970, Gordon & Cato 1972). These lines were initially referred to as the "Galactic Ridge Recombination Lines" (Gottesman and Gordon 1970, Gordon & Gottesman 1971, Jackson & Kerr 1971, Gordon & Cato 1972, Mathews, Pedlar & Davies 1973, Jackson & Kerr 1975, Mebold et al. 1976). Subsequently this RRL emitting gas has been systematically observed near 1.4 GHz by Hart & Pedlar (1976b), Lockman (1976, 1980), Cersosimo (1990) and recently by Heiles et al. (1996b). RRLs from this gas were also observed by Anantharamaiah (1985a, b) near 325 MHz using the Ooty Radio Telescope. Combining his observations with those near 1.4 GHz, Anantharamaiah (1985b, 1986) obtained constraints on the physical properties of the ionized gas. He showed that the density of the ionized gas should be in the range $0.5 - 6$ cm^{-3} .

1.3.2 Continuum Absorption towards Discrete Sources at $\nu <$ 100 MHz

Observations of discrete sources with $b < 10°$ at frequencies of 10 MHz and 22 MHz (Bridle 1969, Roger, Bridle & Costain 1973) and observations of many supernova remnants with $|l| < 40°$ at 80 MHz (Dulk and Slee 1972) show a decrease in their flux densities compared to an extrapolation from high frequency results. These "turnovers" in the continuum spectrum, as shown in Fig. 1.2, are most likely due to free-free absorption by thermal plasma along the line of sight. Dulk & Slee (1975) used observations near 160 MHz and 80 MHz towards several galactic supernova remnants to study the properties of the ionized clouds producing absorption. They argued that the ionized gas producing diffuse, weak RRL emission, detected by Gottesman & Gordon (1970), are

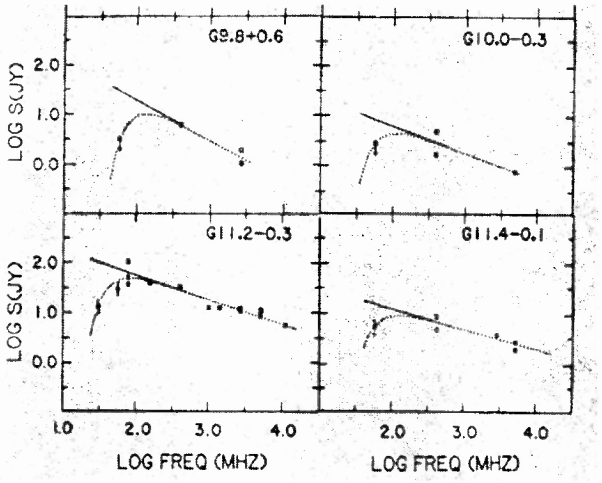

Figure 1.2: Continuum spectra of some galactic supernova remnants taken from Kassim (1989). The observed points and the fitted spectra (dotted line) are shown. The source names are marked on each frame. The spectra clearly shows turnovers at frequencies less than 100 MHz.

responsible for the absorption. Combining their observations with flux measurements at frequencies > 400 MHz, Dulk & Slee (1975) derived the free-free optical depth of the ionized gas at 80 MHz. From the derived optical depth and assuming a temperature of 10^4 K and a size of 30 pc (based on the argument that the gas covered the supernova remnants), they derived $n_e \sim 10$ cm^{-3} . Similarly, using flux measurements towards many other supernova remnants near 30 MHz, Kassim (1989) also came to the conclusion that the absorption is produced by low density ionized gas in the ISM. Kassim (1989) showed that the physical properties of the ionized gas derived by Anantharamaiah (1985b) using RRL observations can indeed account for the continuum absorptions seen towards supernova remnants.

1.3.3 Absorption of the Galactic Non-thermal Background Emission at $\nu < 100$ MHz

Analysis of the observations of the galactic background continuum emission in the frequency range 10 MHz to 4080 MHz show spectral index variation from position to position. These variations in the spectral index were interpreted as due to a mixture of thermal and non-thermal emission by Westerhout (1958) and Mathewson, Healey & Rome (1962). The thermal component manifests as absorptions of the non-thermal background at frequencies < 100 MHz and was apparent in all the low frequency continuum surveys (e.g. Shain, Komesaroff, Higgins 1961). Many of the large ($1^\circ - 2^\circ$) absorption features show spatial correlation with optical H II regions (Shain et al. 1961, Dwarakanath 1989). Dwarakanath (1989) suggests that these absorptions are due to nearby (< few kpc) ionized gas with density ~ 8 cm^{-3} . By combining radio and *IRAS*

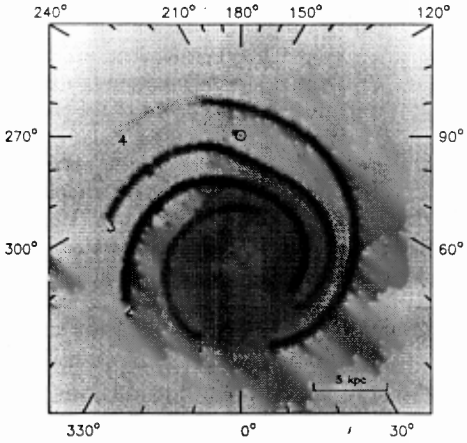

Figure 1.3: Gray scale representation of the free-electron density in the galactic plane, according to the model of Taylor & Cordes (1993). The annular distribution of electrons responsible for the enhanced scattering in the inner Galaxy can be seen in this diagram in addition to the spiral arm and the uniform components.

60μm data. Broadbent, Haslam & Osborne (1989) showed that a significant fraction of the thermal component is associated not only with the compact H II regions but also with an extended low-density gas.

1.3.4 Enhanced Scattering of Radio Waves in the Inner Galaxy

Presence of a turbulent ionized medium in the path of propagation of radio waves produces scattering, resulting in scintillation and angular broadening of radio sources. Scintillation and pulse broadening of pulsar signals, angular broadening of compact extragalactic radio sources and galactic OH masers due to ionized matter in the ISM have been observed. These observations have been used to study the turbulence characteristics, such as the spectrum of the electron density fluctuations, strength of scintillation and its variation with position in the Galaxy. Observations of interstellar scintillation near the galactic plane show that the electron density fluctuations in the ISM are significantly enhanced in the longitude range $|l| < 50°$ at latitudes $< 5°$ (Rao & Ananthakrishnan 1984, Dennison et al. 1984, Cordes, Weisberg & Boriakoff 1985). Models of electron density distribution in the Galaxy have been developed on the basis of dispersion, distance and scattering measurements of pulsars and other radio sources. All these models require a clumped, highly scattering component in the inner Galaxy with a scale height of 150 pc and mean electron density (at $z = 0$) of 0.2 cm^{-3}. This higher density component is necessary to account for the observed enhancement in interstellar scattering in the inner Galaxy (Cordes et al. 1991). A recent electron density distribution model in the Galaxy derived by Taylor & Cordes (1993) is shown in Fig. 1.3. In this model, the clumpy inner Galaxy component is modeled as an annular distribution

of free electrons as shown in Fig. 1.3. Apart from the inner Galaxy component this model also has a nearly uniform, moderately-scattering component with a scale height ≥ 1 kpc and a large filling factor (> 0.5) and a spiral arm component, which is mostly due to H II regions in the spiral arms. While the moderately-scattering component is identified as the WIM, there is no consensus regarding the origin of the clumpy component. Based on the derived scale height, filling factor and the annular shape of the inner Galaxy component, it has been suggested that this component is associated with star forming regions or H II regions or supernova remnants in the inner molecular ring (Taylor & Cordes 1993). On the other hand Rao & Ananthakrishnan (1984), Dennison et al. (1984) and Anantharamaiah & Narayan (1988) have associated it with the low-density ionized gas responsible for the RRL emission in the inner Galaxy. Based on VLBI (Very Long Base Line Interferometry) observations of compact radio sources in the Cygnus regions Spangler & Reynolds (1990) also favored the latter suggestion.

1.3.5 Evidence from C II 158μm and N II 205μm Lines

Interstellar gas cools mainly through radiative transitions. Two important cooling transitions of the ISM are the N II 205 μm and C II 158 μm fine structure lines. The ionization potential of nitrogen is 14.5 eV and hence the N II 205 μm originates in regions where hydrogen is fully ionized. On the other hand, since the ionization potential of carbon is 11.3 eV, carbon atoms can be ionized even in regions where hydrogen is neutral. Thus ionized carbon is present both in neutral and ionized components of the ISM. Observations of the cooling transitions N II 205 μm and C II 158 μm can thus trace the presence of ionized gas in the ISM. The critical densities of the ionized gas for these line emissions are ~ 150 cm^{-3} and ~ 30 cm^{-3} for N II and C II respectively when the temperature is ~ 7000 K. A survey of C II and N II lines conducted by the FIRAS (Far Infrared Absolute Spectrophotometer) instrument in the *COBE* (Cosmic Microwave Background Explorer) satellite has detected lines from almost all directions in the galactic interior (Wright et al. 1991). This survey has an angular resolution of $7^\circ \times 5^\circ$. Recent high resolution survey by balloon borne instrument in the galactic plane also give similar results (Nakagawa et al. 1998). The critical density for N II line emission falls at the lower end of the densities for normal H II regions. Petuchowski & Bennett (1993) therefore suggested that, most of the N II emission originate from low-density ionized gas in the ISM. The possible sites of the origin of the C II lines observed by *COBE* have been discussed by Petuchowski & Bennett (1993) and Heiles (1994). While the first author argues that the C II line originates predominantly from the neutral regions, Heiles (1994) has suggested that the low-density ionized gas is a strong contender.

1.4 Origin of the Low-density Ionized Gas in the Galactic Disk

The origin of low-density ionized gas discussed in the previous section is not completely understood although there are several suggestions regarding it. We summarize the three prevalent models.

Evolved H II regions : Mathews et al. (1973) have used RRL and continuum emission near 1.4 GHz in the longitude range $l < 48^\circ$ to estimate the properties of the

ionized gas producing RRLs. They derived temperature and density for the line emitting region as $\sim$ 6000 K and $\sim$ 2 cm^{-3} respectively. These regions have an angular extent of $\sim$ 3° – 5°. Based on these estimates, they suggested that the ionized gas responsible for low frequency RRL emission are extended low-density H II complexes similar to NGC2244, NGC7000 and NGC7822. Multifrequency cm-wave RRL observations towards a set of directions in the inner Galaxy were used by Shaver (1976) to constrain the physical properties of the ionized gas producing line emission. Analysis of these observations indicated that in most cases the ionized gas should have electron densities of 5 – 10 cm^{-3} and diameters of 20 – 150 pc with relatively high temperature (> few 1000 K). Based on these derived parameters, Shaver (1976) also suggested that the gas responsible for line emission were the large low-density H II regions.

Galactic O stars are usually associated with the "compact radio" H II regions which are bright in radio continuum. However, Mezger & Smith (1975) found that only 10 – 20 % of all O stars in the Galaxy are embedded in such H II regions. Most of the Lyman continuum photons emitted by the O star in these H II regions get absorbed by the gas and dust within the H II regions. The remaining large fraction of bare O stars can ionize and thus produce extended low-density H II regions (Mezger 1978). Mezger (1978) suggested that the low-frequency RRLs originate from these evolved low-density H II regions.

Envelopes of normal H II regions : Earlier low frequency RRL surveys in the galactic plane have detected lines in almost all positions in the longitude range $l < 40°$ (Hart & Pedlar (1976b),Lockman 1976, Anantharamaiah 1985a). This longitude range is also rich in normal H II regions which is evident from their presence in large numbers as bright continuum sources near 5 GHz (e.g. Downes et al. 1980) at $l < 40°$. The central velocities of the observed H110α emission from normal H II regions correlate well with low frequency lines detected in the same directions (Lockman 1980, Anantharamaiah 1985a). The distribution of low frequency line emission as a function of galactocentric distance is also similar to that obtained from the H110α emission from normal H II regions (Anantharamaiah 1986). These facts indicate that the low frequency RRL emission is associated with known normal H II regions. The low frequency lines, however, cannot originate in the normal, higher density (> 100 cm^{-3}) H II regions themselves owing to pressure broadening and continuum opacity effects. The estimated physical properties of the ionized gas producing low frequency RRLs are in the range $n_e \sim 0.5$ – 6 cm^{-3} , size $\sim$ 50 – 300 pc and $T_e \sim$ 3000 – 8000 K (Anantharamaiah 1985b). These estimates and the correlation in the velocity and distribution led to the suggestion that the ionized gas responsible for low frequency RRLs are low-density outer envelopes of normal H II regions (Lockman 1980, Anantharamaiah 1986). A similar suggestion was made by Hart & Pedlar (1976a) based on their study of H II region complex W3, where evidence of association of extended low-density gas was seen from their H166α observations.

A recent study by Heiles et al. (1996b) of thermal gas in walls of cavities in the galactic gaseous disk formed by clustered supernovae, called "worms", have detected low frequency (1.4 GHz) RRL emission from them. The walls of these cavities are ionized by photons from the hot stars in the cluster whose supernovae originally produced them. It has been estimated that about 17 % of the diffuse low frequency RRL emission originate in the walls of these"worms" (Heiles et al. 1996b). The morphology of such "worms" can also be classified in the H II –envelope picture (McKee & Williams 1997).

ELDWIM : While suggesting that evolved low-density H II regions were responsible

for low frequency RRL emission (see above), Mezger (1978) also pointed out that the size of these objects were large enough for their Strömgren spheres to partially overlap. He has referred to this ensemble of evolved H II regions as an extended low-density gas. This picture was further developed by Petuchowski & Bennett (1993) while interpreting the N II 205μm observations in the galactic plane by *COBE* FIRAS. They suggested a model where the extended low-density ionized gas is conflated with the well known WIM and referred to it as the "extended low-density warm ionized medium". In this model the $< n_e^2 >$ of the WIM becomes large enough in the galactic interior to produce diffuse low frequency RRL emission. This enhanced density version of the WIM forms a pervasive medium in the inner Galaxy (Heiles 1994, Heiles et al. 1996b).

1.5 A preview of the present Work

This thesis presents an extensive survey of RRLs at frequencies near 327 MHz from the galactic plane using the Ooty Radio Telescope and an interpretation of the data in terms of the physical properties of the ionized gas, its distribution in the galactic disk and association with other components. It is a follow up to the study by Anantharamaiah (1985a) towards a selected set of directions using the ORT. Following the first observations by Gottesman and Gordon (1970) of RRLs near 1.4 GHz from a distributed low-density ionized component in the galactic plane, there have been several surveys. These surveys were made near 1.4 GHz in the galactic plane ($|b| < 0°.5$) and mostly in the longitude range $l < 50°$ (e.g. Lockman 1976). Lines were detected in almost all positions observed in this longitude range. But these surveys have two limitations: (a) most of the observations were made at a single frequency near 1.4 GHz and (b) none of the observations form a complete sampling of any region of the galactic plane. However, in order to determine the physical properties of a line emitting regions it is necessary to have RRL observations at more than one frequency. Also a complete sampling of the line emitting region will give a clearer picture of the distribution of the low-density ionized gas in the galactic plane. Therefore we undertook an extensive survey of RRLs near 327 MHz.

Any large scale survey of low frequency RRLs is a time consuming endeavor since the line emission is very weak, requiring many hours of integration at each position. To reduce the observation time, we built a special multi-line spectrometer. This multi-line spectrometer is capable of simultaneously observing all the four RRL transitions inside the frequency band of operation of the ORT. These are adjacent transitions and hence the spectra can be averaged to improve the signal to noise ratio thus reducing the observation time by a factor of four. A brief description of the ORT, the details of the receiver system and the data reduction procedures are described in Chapter 2.

The ORT, when used in the normal mode has a beam width of $\sim 2°$ along right accession (RA) and $\sim 5'.5 \sec(\delta)$, δ being the declination, along declination. The declination coverage of the telescope is limited to $\pm 40°$ when observed in this mode. Thus two strips of the galactic plane can be observed covering the longitude range $l =$ 332° to 0° to 89°, which is towards the inner Galaxy, and $l = 172°$ to 252°, which is in the outer Galaxy. To completely sample the observable portion of the Galaxy with a beam of $5'.5$ would require an enormous amount of telescope time even with the new receiver system. We therefore adopted a two fold strategy for these observations.

(i)*Low Resolution RRL survey* : If the regions to be surveyed are smooth and extended, then the observation time can be considerably reduced without loss of infor-

mation by using lower angular resolution. Use of low resolution without too much loss of information is possible in the present case since earlier studies (mentioned above) have shown that low density regions are extended in the galactic plane. For extended objects, the sensitivity of the observations does not depend on the collecting area of the telescope as long as the object fills the primary beam. We therefore decided to conduct a survey using a portion of the ORT, called a 'module', which has a beam width of $\sim 2^\circ \times 2^\circ$. The objectives of these observations are:

1. To study the distribution of ionized gas and its association with other components of the ISM.

2. To compare the RRL emissions in the inner and outer Galaxy and also to determine the latitude extent of line emission.

3. To estimate the physical properties of the ionized gas by combining the data with observations at other frequencies.

4. To compare with other observations which show evidence for the presence of extended low density ionized gas, e.g. *COBE* FIRAS observations of N II and C II line emission.

In this low-resolution mode, we made a complete sampling of the inner galactic plane in the longitude range $l = 332^\circ$ to 0° to 89°. RRLs were detected in almost all directions in the inner Galaxy. Although the resolution is coarse, these observations are the first complete sampling of this longitude range. The outer Galaxy was sampled at 14 positions equally spaced in longitude. This coarse sampling was chosen because previous observations have shown that the line emission in the outer Galaxy is not as wide spread as in the inner Galaxy. We have detected lines at only three positions in the outer Galaxy. Observations along the latitude were made over $b = \pm 4^\circ$ at two specific longitudes, $l = 0^\circ$ and $13^\circ.9$. Lines were detected up to $\pm 3^\circ$.

In Chapter 3, we describe the low resolution survey, present the results and describe the general characteristics of the data. The distribution of the low-density gas in the galactic disk as derived from the central velocity and width of the observed lines in the survey, scale height of line emission and analysis of the observations in the outer Galaxy are presented in Chapter 4. To study the association of this line emitting region with other components of the ISM, such as H II regions, WIM and molecular gas, we compare their derived distributions. This comparison is also discussed in Chapter 4. In Chapter 5, we derive the properties of the line emitting region by combining the observations presented in Chapter 3 with data at other frequencies taken from available literature. The theory used for interpreting the RRL data in terms of the physical properties of the line emitting region is also given in Chapter 5. The derived physical properties are then used to compute the C II 158 μm and N II 205 μm line intensities and the free-free absorption of the galactic non-thermal emission near 35 MHz due to this gas. These computations and comparison with observations are also presented in Chapter 5.

(ii)*Full telescope observations* : A selected set of 2° and 6° fields in the inner Galaxy are further observed with a $2^\circ \times 6'$ beam obtained using the full ORT. The fields that are observed in this mode are positions where RRLs were detected in the low resolution survey. Our objectives are to determine the angular structure of RRL emission, if any, using a finer resolution and compare the average spectra over a 2° area with that

obtained in the low resolution survey in the same directions. These observations and results are discussed in Chapter 6.

In Chapter 7 we used the derived distribution of the ionized gas, its association with other components of the ISM and the estimated physical properties to evaluate the possible origin of the low-density ionized gas that is responsible for the observed low frequency RRL emission. Analysis of the survey data shows that the distribution of RRL emission near 327 MHz is similar to star forming regions in the galactic disk. Based on several considerations and also the derived physical properties, we favour the suggestion that the low-density ionized regions are mostly envelopes of normal H II regions. These low-density ionized regions do not form a pervasive medium in the inner Galaxy as implied by the term Extended Low-density Warm Ionized Medium (ELDWIM).

In Chapter 8, we summarize the observations and results discussed in this thesis.

Chapter 2

Technical Aspects – the Telescope, the Multi-line Spectrometer, Observing Procedure and Data Reduction

2.1 Introduction

All the observations presented in this thesis were made using the Ooty Radio Telescope (ORT). In 1993, the front-end receiver system of the telescope was upgraded with a low noise amplifier ($T_{amp} \sim 50$ K) followed by a microstripline phase shifter (Selvanayagam et al. 1993). This new system improved the sensitivity of the telescope by a factor of two compared to the earlier system. A computer controlled declination setting and monitoring system was also implemented along with the front-end upgrade. The new system with its enhanced stability and sensitivity motivated us to undertake an extensive RRL survey using the ORT. Even with the increased sensitivity, a large scale survey of RRLs is time intensive since the strength of the spectral lines are typically $\sim 10^{-3}$ times the system noise. To reduce the observation time, a multi-line Spectrometer which can simultaneously observe all the four RRL transitions that occur within the receiver bandwidth of the ORT was built. These four adjacent transitions are averaged to improve the signal-to-noise ratio by a factor of two thus reducing the observing time by a factor of four. A further reduction in observing time by a factor of two is achieved by having two such spectrometers each observing all the four RRL transitions either from adjacent positions of the sky or the same position of the sky with two "modules" of the telescope. The new back-end, utilizes an existing spectrometer and the technique of 'recirculation' to create the equivalent of eight simultaneous spectrometers. When compared with the earlier system the overall reduction in observing time is a factor of 16.

In this chapter, we present a brief description of the ORT and a detailed description of the new back-end, the data acquisition system, observation modes, and the data reduction procedure. We also discuss the sensitivity of the observations, measurement of continuum antenna temperature and calibration of the spectrum.

2.2 Ooty Radio Telescope

The ORT is a 530 m × 30 m off-axis parabolic cylinder operating at a nominal center frequency of 326.5 MHz (Swarup et al. 1971). An array of 1056 half-wave dipoles in front of a 90° corner reflector forms the primary feed of the telescope. This feed system essentially operates as a broadside phased array and is oriented along the north-south (NS) direction. The telescope can be mechanically rotated in the east-west (EW) direction. The rotation axis is inclined to the local horizontal by an angle equal to the latitude of the place, thus making the telescope equatorially mounted. In the NS direction, the telescope response is steered electronically by introducing a suitable phase and delay gradient along the dipole array.

The front-end receiver system consists of a low noise amplifier (T_{amp} = 50 K) and a strip line diode-switch controlled phase shifter following each of the 1056 dipoles. The signals received by groups of 48 dipoles are added in-phase. There are 22 such groups, which are called "modules" and designated as N1 to N11 northern modules and S1 to S11 southern modules. The signal received by each of the modules is down-converted to an intermediate frequency (IF) of 30 MHz by mixing with a local oscillator (LO). The LO is distributed to all modules on equal length cables from a common source. At this stage, the bandwidth of the receiver system is restricted to $\sim$ 15 MHz. The IF signals are brought to the receiver room through equal length cables. The response of each module is steered by applying a phase gradient across the 48 dipoles by using the phase shifters which are controlled by a computer in the telescope control room. The beam width (FWHM) of each module is 2°.3 in EW and 2°.2 sec(δ) in NS, δ being the declination. The beam width depends on the declination since the projected area changes with declination.

In the "total power" configuration, the outputs of the 22 modules are combined in the receiver room, after passing the signals through a delay compensation network, to produce 12 beams, each having FWHM $\sim$ 2°.3 × 5′.5 sec(δ), δ being the declination. The delay compensation network compensates the geometric path difference between signals from different modules. The twelve beams are spread along the NS direction and are separated by 3′sec(δ). They are designated as Beam 1 to Beam 12, Beam 1 being the south most beam. To form these beams, the signals from the modules are in fact combined in two steps – first all the north and south modules are separately combined to form twelve north and south beams; then the corresponding north and south beams are either added or multiplied to form the 12 total power or correlation beams.

The method of steering the telescope in the NS direction has been discussed in detail by Ananthakrishnan (1976) and Singal (1988). Here we focus on the implementation of a new local oscillator phase shifter which improved the electrical phasing of the telescope over the entire 15 MHz bandwidth. This new LO-phase shifter is now a part of the normal declination setting procedure. The basic principle involved is the following and is illustrated in Fig. 2.1. For observing a source at a declination δ, the response of the individual 22 modules are tilted by applying a phase gradient across the dipoles in the modules. Since the delay due to geometric path difference between modules are larger than the decorrelation time (approximately equal to the inverse of the bandwidth), the delay should be compensated before combining the signals from different modules. These delays are compensated by introducing cables in the IF (intermediate frequency) path. The resulting change in the IF pathlength, produces a residual phase difference. In the earlier system, the delays were compensated to an accuracy of $\lambda_{IF}/(2c')$, where

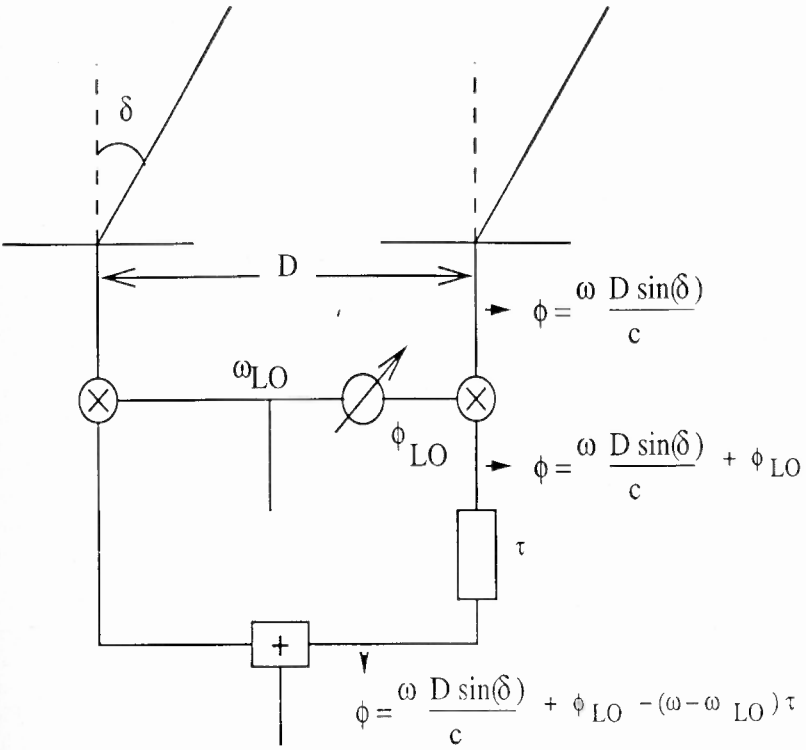

Figure 2.1: Schematic diagram illustrating how signals received by two of the 22 modules of the ORT are combined. Note that the delay (τ) is compensated in the IF path. The phase (ϕ) of the signal at a module with respect to the other at different stages are marked. Here D is the distance between the modules, δ is the declination, c is the velocity of light, ω is the angular frequency of the signals received, ω_{LO} is the local oscillator frequency (in radian/sec) and ϕ_{LO} is the phase introduced in the local oscillator path. If $\tau = \frac{D sin(\delta)}{c}$ then the residual phase at the final combiner is $\phi_{LO} + \omega_{LO}\tau$, which can be removed by choosing $\phi_{LO} = -\omega_{LO}\tau$.

λ_{IF} is the IF wavelength and c' is the velocity of light in the cable. The residual phases were adjusted using cable lengths in units of $\lambda_{IF}/64$. In the the new LO-phase shifter system, the delays are compensated to an accuracy of $\lambda_{IF}/(64c')$ and the residual phases are adjusted by changing the phase of the local oscillator signal.

For the spectral line work with the ORT, all the four RRL transitions within the 15 MHz bandwidth were observed simultaneously (see below). Thus the LO-phase shifter system is essential for these observations to ensure better electrical phasing of the telescope over the entire bandwidth. The improved electrical phasing gives similar sensitivity in all the four recombination line bands.

2.3 Spectral Line Receiver System

The nominal center frequency of operation of the ORT is 326.5 MHz and the bandwidth of the receiver system is $\sim$ 15 MHz. In this frequency range there are four recombination lines corresponding to $\Delta n = 1$ transition to states with principal quantum numbers n = 270, 271, 272 and 273. The rest frequencies of hydrogen lines corresponding to these transitions are 332.25366 MHz (H270α), 328.59586 MHz (H271α), 324.99155 MHz (H272α) & 321.43973 MHz (H273α) and that of the carbon RRLs are 332.41943 MHz (C270α), 328.75980 MHz (C271α), 325.15372 MHz (C272α) & 321.60004 MHz (C273α). By observing all the four transitions simultaneously and averaging the spectra, the observing time is reduced by a factor of four. A new spectral line receiver was built with the objective of observing all the four RRL transitions (both hydrogen and carbon) simultaneously. In fact when we designed the new system to adopt to an existing spectrometer, it turned out that the new receiver could simultaneously observe eight transitions. We describe below (Section 2.4.1) how the new receiver system was used to simultaneously observe two sets of four transitions to reduce the observing time by a further factor of 2.

In the new spectrometer, each of the RRL transitions can be observed with a bandwidth of $\sim$ 750 kHz and a frequency resolution of $\sim$ 1 kHz. The reference spectrum is measured by frequency switching. The new multi-line receiver system was built around an already existing 512 channel auto-correlation spectrometer, described by Subrahmanyan (1989). The overall block diagram of the new spectrometer is given in Fig. 2.2. The first stage of the analog system is a power combiner which has a bandwidth of 15 MHz. The signals from the telescope are connected at the inputs of this stage (I/P1 to I/P4). The rest of the system takes the combined output and produces two sets of four baseband signals containing the four RRL transitions. The eight baseband signals from the analog system are sampled and their autocorrelation functions are measured by the recirculator and the spectrometer. The autocorrelation values are read from the spectrometer by the data acquisition computer. A frequency synthesizer which generates the first LO is controlled by the same computer. To measure the reference spectrum the first local oscillator is switched at a rate of 1 second by the computer. In the subsequent discussion we explain each block of the spectrometer system in some detail.

2.3.1 Autocorrelation Spectrometer

The details of the original one-bit autocorrelation spectrometer are given in Subrahmanyan (1989). The information relevant for subsequent discussions here are as follows. The autocorrelation spectrometer operates at a clock frequency of 18.432 MHz

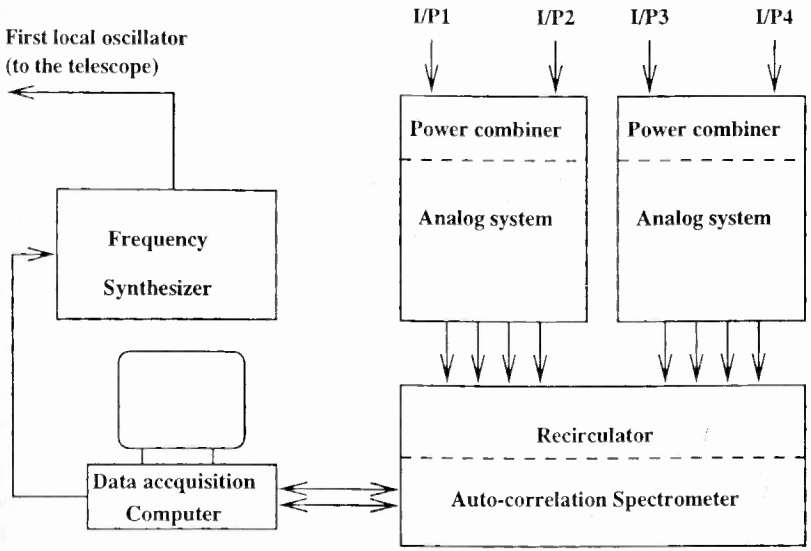

Figure 2.2: Block diagram of the spectral line receiver system.

and consists of 512 delay segments which are grouped in multiples of 32 correlators. Each correlator is followed by an integrator. For the recirculator, the delay segments are rearranged into eight groups each consisting of 64 delay lines and corresponding correlators and integrators. Each of these groups can measure the autocorrelation of a one-bit time series up to a maximum of 64 lags. The integrators are 31 bits long. The integration times are such that the total counts do not exceed 23 bits. The most significant 16 of the bits are read which results in a truncation of 7 bits. The error due to this truncation is less than the statistical fluctuations of the correlation counts if the integration time is $\gg 4$ msec (see Subrahmanyan 1989).

2.3.2 Recirculator

The bandwidth and spectral resolution required for observing RRL transitions are about 750 kHz and 1 kHz respectively. The autocorrelation spectrometer thus requires about 750 correlators to obtain the required spectral resolution. If the 750 kHz frequency band is sampled at the Nyquist rate, then the data rate is much smaller compared to the maximum clock frequency of operation of the spectrometer. This fact can be utilized to "recirculate" the data multiple times through the existing set of 64 correlators for measuring the autocorrelation over a larger number of lags and thus obtain the required spectral resolution.

We adopted the following hardware design scheme for the recirculator. The sampling frequency of the input data is chosen to be 12 times slower than that of the clock frequency of the spectrometer i.e. $18.432/12 = 1.536$ MHz. This allows a maximum

bandwidth of 768 kHz which is sufficient for observing the RRL transitions. Since the spectrometer can operate 12 times faster than the sampling rate, the sampled data can be recirculated 12 times through one group of 64 correlators resulting in correlations up to 768 lags (i.e. 64 × 12). The resulting spectral resolution is 1 kHz. Since the correlator is already configured to process 8 sets of 64 channels parallelly it is possible to process simultaneously 8 baseband signals, each with a bandwidth of 768 KHz. Analog systems (i.e. baseband converters and filters) were arranged such that these 8 basebands corresponds to two sets of the four RRL transitions which occur within the Ooty band. The total number of spectral channels obtained by the above method of recirculation is 6144 (i.e. 768 × 8).

A block diagram of the digital system is given in Fig. 2.3. The hardware configuration can be divided into eight identical groups. Each group consists of a sampler, a "dual memory" bank, two multiplexers and a set of 64 correlators. The analog data is sampled at 1.536 MHz and quantized to one-bit by the sampler. The one-bit time series are stored in the "dual memory" bank. In Fig. 2.3 the memory bank of the first group is labeled as M1a and M1b. The dual memory bank allows a continuous flow of data by writing into one set of memory while the other is being read. The size of each memory is 192 Kbytes. This is chosen so that the time required to fill the memory bank with the input data is approximately the rate at which reference spectrum should be measured. For a memory size of 192 Kbytes, the total time is 1.024 sec, which gives an optimum rate for frequency switching. The control signal which switches the two memory banks also goes to the data acquisition computer to switch the local oscillator frequency for measuring the reference spectrum.

Each memory bank is written until it is full. Then the memory bank is switched and the writing continues into the second bank. At this time, the data from the filled memory bank is now read at a clock rate of 18.432 MHz and fed to a group of 64 correlators. There are two inputs to each of the 64 correlator group: one input has a direct path to the multipliers (designated as "undelayed" in Fig. 2.3) and the other input passes through the 64 delay lines (designated as "delayed" in Fig. 2.3). In the first cycle, the recirculator feeds identical samples to the two inputs. Thus the spectrometer measures the correlation from 0 to 63 lags averaged over 1572864 (i.e. 192 × 8 × 1024) one-bit samples in the first cycle. In the second cycle, data in the "undelayed" path is same as in the first cycle but in the "delayed" path, data with an offset of 64 samples is fed in. This delay is achieved by offsetting the read address of the memory. This offset is equivalent to introducing a delay of 64 lags. Thus in the second cycle, the same 64 correlators measure correlation for lags 64 to 127. This sequence is repeated 12 times with offsets in the read address in multiple of 64. At the end of 12 cycles, the correlations span 0 to 767 lags. At the end of each cycle, the correlations are read from the spectrometer by the data acquisition computer. Each cycle takes about 85.3 msec (i.e. $1572864/(18.432 \times 10^6)$). This means that at the end of 12 cycles, the memory bank into which the data is being written will be full. The memory banks are then switched and the whole operation is repeated. These operations are carried out simultaneously in all the eight groups of 64 correlators thus processing all the eight analog signals.

2.3.3 Analog Back-end

A block diagram of the analog back-end is shown in Fig. 2.4. The beam forming network (see Section 2.2) of the ORT combines the IF signals from all the north and

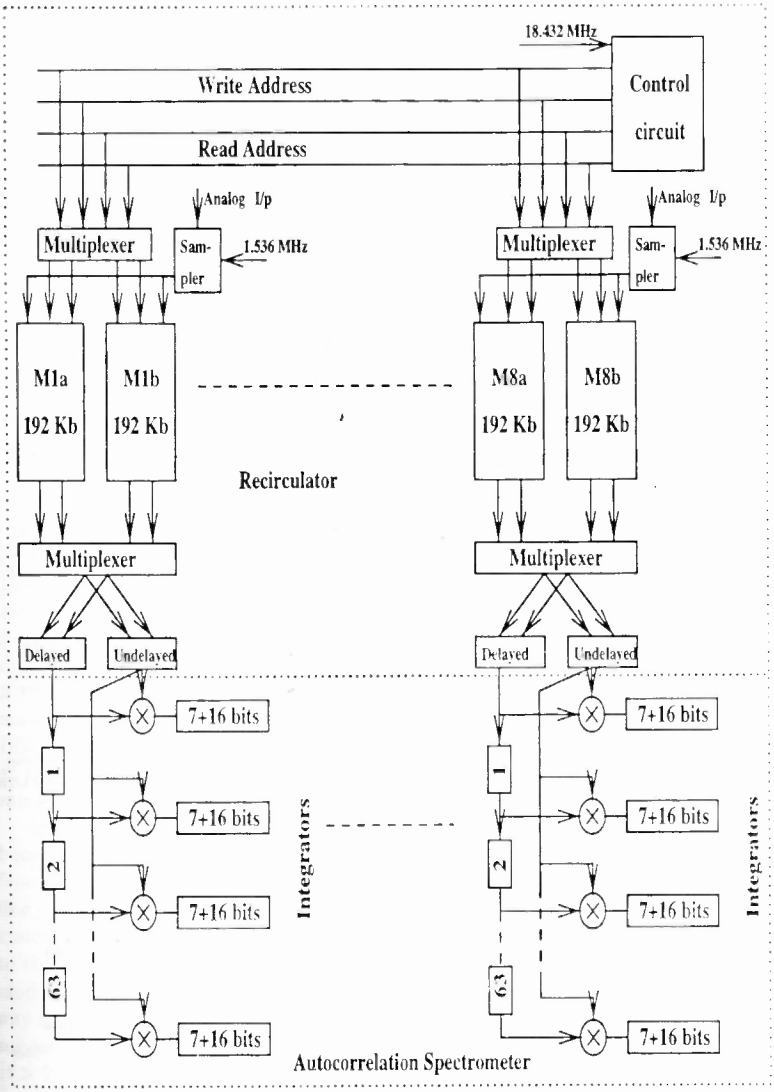

Figure 2.3: Detailed block diagram of the Recirculator.

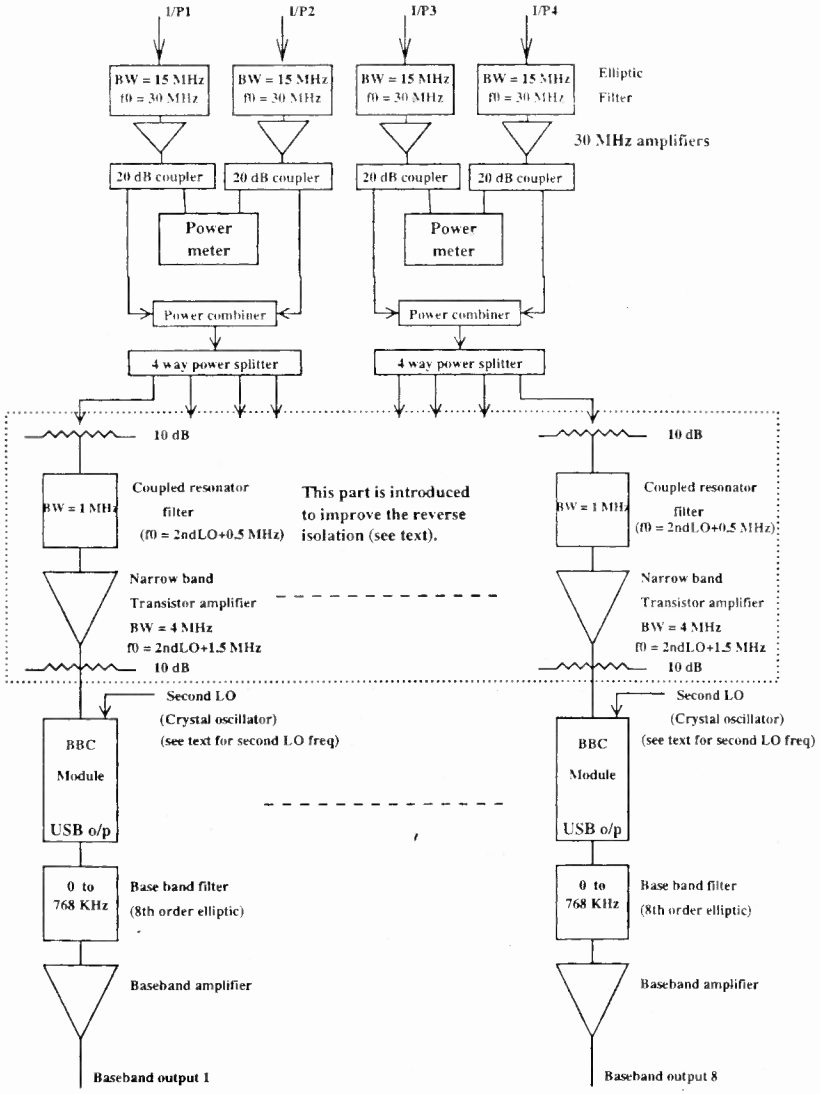

Figure 2.4: Block diagram of the analog back-end of the spectral line receiver.

south modules separately for twelve different beams and these combined signals are available for further use. To get the full spatial resolution of the telescope, these signals have to be added in phase. Before adding the signals, the gains of the North and South half of the telescope are equalized. The gains are adjusted using a power meter which is connected through a 20 dB coupler following the amplifier. A broadband (> 15 MHz) power combiner adds the signals from the north and south half of the beams that are used for observations. The power combiner is followed by a 4 way power splitter which produces four copies of the 15 MHz frequency band centered around 30 MHz. There are two such systems corresponding to two of the 12 beams thus giving a total of eight outputs. The rest of the analog system is identical for each of the eight outputs.

The output of the 4 way power splitter is followed by an amplifying stage with high reverse isolation (~ 65 dB). The need for high reverse isolation is explained below. The four RRL transitions appear at the IF frequencies 35.83655 MHz, 32.17783 MHz, 28.57263 MHz and 25.01987 MHz (these are the mean of the rest frequencies of hydrogen and carbon transitions when translated to the IF band) when down-converted with the nominal first local oscillator frequency of 296.5 MHz. A narrow band coupled resonator filter tuned to each of the four RRL transitions inside the IF band restricts the bandwidth of the subsequent stages to 1 MHz. The filters are followed by narrow band (4 MHz bandwidth) transistor amplifiers. To improve the reverse isolation further, two 10 dB attenuators as shown in Fig. 2.4 are also introduced. The output of the amplifiers are fed to baseband converters (BBC). We used the BBC modules designed for the Giant Meter Wave Radio Telescope. The BBC modules takes a local oscillator (we refer to this as the second LO) along with the IF signal as its input and translates the frequency components in the IF band above and below the second LO to two basebands, the Upper Side Band (USB) and Lower Side Band (LSB) respectively. The maximum bandwidth of each of the sidebands is about 16 MHz. We have chosen 35.2327 MHz, 31.5777 MHz, 27.9738 MHz and 24.4337 MHz as the four second LOs, which are generated by custom made crystal oscillators. Thus the RRL transitions appear in the USB outputs of the BBCs. An anti-aliasing, eighth order elliptic filter with a sharp roll-off is introduced at the output of the BBC followed by a baseband amplifier. These outputs go to the samplers.

In the original design of the analog system, there was only one broadband amplifier between the output of the 4 way splitter and the BBC module. This system with four variable second LOs was to be used for extragalactic RRL observations where the line separation changes due to redshift. However, initial test observations with the system showed spurious narrow band signals in the spectra. This was tracked down to the leakage of the second LOs from the BBC modules which then produced inter-modulation products. To prevent the second LO signals from leaking back to the 4 way splitter, we modified the system as follows. (I thank A. J. Selvanayagam for this suggestion.) Each of the narrow band filters were designed to produce an attenuation of > 20 dB at the second LO frequencies used in the other three BBCs. The transistor amplifiers have a reverse isolation > 20 dB, thus improving the overall isolation. The two 10 dB attenuators, whose loss is compensated by the amplifier, also adds up to a total isolation of > 60 dB. (This scheme was later replaced by a broad-band high reverse isolation stage. However all the observations described in this thesis were made with the system described above.)

2.4 Observing Procedure

A parameter file consisting of the source name, its B1950 coordinates, observing date and time, precessed coordinates, LSR velocity of the source, any required velocity offset, observation duration, mode of observation (see Section 2.4.1), configuration of the spectral line receiver system, and other relevant information is created before each observing session. As described earlier, the first LO is controlled by the computer and hence its frequency can be suitably adjusted to position all the four RRL transitions within the corresponding basebands. At an observing frequency near 327 MHz, Doppler shift of the spectral line due to change in LSR velocity of the telescope over the observing time is less than the frequency resolution of the spectrometer. Therefore no on-line velocity correction is applied. The specified LSR velocity of the source, the velocity offset and the computed LSR velocity correction are used to set a first LO frequency such that the spectral line appears at a preassigned reference channel. The computed LO frequency is included in the parameter file. The reference spectrum is measured by switching the first LO. The frequency to which the first LO should be switched is also specified in the parameter file. For all the observations, we have used an offset LO frequency such that the spectral line shifts between two halves (i.e. 384 MHz each) of the baseband. This is equivalent to the Dicke switching scheme (Dicke 1946) which maximizes the signal-to-noise ratio (SNR) for a given observing time. Before starting the observations, all the potential sources of interference within the observatory were switched off.

2.4.1 Observation modes : Single Module and Full Telescope Observations

The observations presented in this thesis were done in the two modes discussed below. They are designated as Single Module mode (or Mode A) and Full telescope mode (or Mode B).

1. **Single Module Mode (Mode A) :** As explained in Section 2.2, the ORT is made up of 22 modules. Each module is equivalent to a single telescope of size 30 m $\times$ 23 m and has a beam width of $2^\circ.3 \times 2^\circ.2 \sec(\delta)$, δ being the declination. In Mode A, the four RRL transitions are observed simultaneously from two such modules. The eight RRL spectra from the two modules are later averaged. The incoherent addition of the signals from the two modules preserves the spatial resolution and under certain conditions increases the SNR by $\sqrt{2}$ (see Section 2.8).

   If the observing source is extended such that it fills the beam of the telescope, then there is no loss of sensitivity even if the beam is large (see Section 2.8). This fact is used in making the low resolution RRL survey of the galactic plane discussed in Chapter 3 where Mode A is used for the observations. Previous observations have indicated that the RRL emission is extended over several degrees. Thus observing them with a beam of $\sim 2^\circ \times 2^\circ$ will not cause any loss of sensitivity.

2. **Full Telescope Mode (Mode B) :** The ORT is used as a single telescope in this mode. The signals from the 22 modules are added in phase to obtain a $2^\circ \times 5'.5 \sec(\delta)$ beam. The beam forming network (see Section. 2.2) produces twelve such beams (labeled 1 to 12) and separated by $3'.3 \sec(\delta)$ in the NS direction. The

four RRL transitions are observed simultaneously from two of the beams (beams 5 and 7) which are separated by $\sim 6'$ (see Section 2.8 regarding the choice of the beams). The finer resolution of $\sim 6'$ in one direction in this mode can be used for studying the angular variation of RRL emission in this scale. These observations are discussed in Chapter 6.

2.5 Data Reduction

The data reduction process consists of several steps such as data examination and editing, interference excision, weighted averaging of the spectra, baseline removal, smoothing and Gaussian fitting. The various steps are discussed below.

The autocorrelation values of few lags (< 0.6 % of the total number of lags) were found to produce "abnormal" values due to a hardware error in the system. About 25 % of the data is affected by this error. Therefore we first examined the autocorrelation values for each basic integration of ~ 1 min and the bad correlation values were replaced by interpolated values from adjacent lags. The on-line and reference spectra were obtained by Fourier transforming the autocorrelation values after applying a hanning weighting function. A difference spectra was constructed for each basic integration. The line emission is generally too weak to detect in this difference spectrum and is dominated by possible baseline curvature. A third order baseline was fitted to the spectrum after excluding the channels where line emission is expected, and the fitted baseline was removed from the entire spectrum.

Individual on-line, reference and difference spectra were carefully examined for interference. A grey scale display of the spectra with the channels along x-axis and time along y-axis with menu driven options for editing them was used for this purpose. Spectra that were badly affected by interference were discarded. Spectra which had narrow band interference in only a few channels were retained but the channels which were affected by interference were given a weight of zero while averaging the spectra. The sum of weights for each channel was separately kept track of until the final spectrum was obtained. This method resulted in slightly different integration times for each channel. Typically the maximum difference in integration time was $< 10\%$.

The eight final spectra and the respective channel weights were then written to a file in a format compatible with the UniPops single-dish spectral line analysis software package, developed by the National Radio Astronomy Observatory, USA. Although UniPops contains almost all the tasks required for single dish spectral line data analysis, it does not support the channel weighting scheme. We have therefore added new "verbs" to this package which takes account of the channel weights. This was achieved by modifying the code for some of the existing "verbs". We also developed several "procedures", which take into account the channel weighting scheme. These procedures make use of the new "verbs" and other standard ones in the package. The data processing steps inside the UniPops package are as follows.

1. The individual spectra were examined further. Channels showing any residual interference were removed by setting their channel weights to zero.

2. As described earlier, the local oscillator frequency was switched periodically for obtaining the reference spectra by half the bandwidth of observations. Hence the expected spectral line appears in both halves of the frequency band. The two

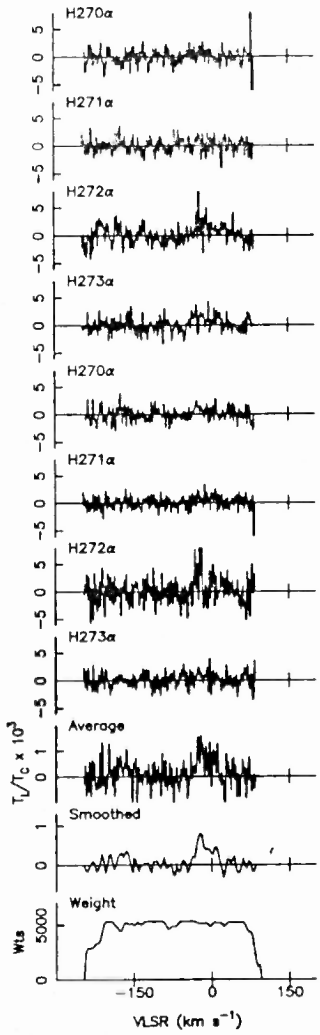

Figure 2.5: The eight "folded" spectra corresponding to the two sets of four recombination lines observed simultaneously using two modules of the ORT towards $l = 345°.5$ and $b = 0°.0$ are shown. The four lines correspond to $\Delta n = 1$ transition to states with principal quantum numbers $n = 270$, 271, 272, 273. The average ('Average') of all the eight spectra, the final spectrum ('Smoothed') obtained after smoothing the average spectrum to a spectral resolution of 8 km s^{-1} and its channel weights ('Weights') are also shown. The y-axis of the spectra is in units of line to continuum ratio (T_L/T_C) and x-axis is in LSR velocity.

halves of each spectra were averaged to get the "folded" spectrum. Any residual base line in the spectrum is removed from each half before "folding".

3. The final spectrum is obtained by averaging all the "folded" spectra after correcting for any velocity offset. The small differences in the velocity resolution of the different spectra (due to different rest frequencies) were ignored. Fig. 2.5 shows a typical set of "folded" spectra obtained from the eight basebands, the corresponding channel weights and the integrated spectrum. Typical effective integration time for the final spectra is 20 hours.

4. The final integrated spectrum is convolved with a box function of appropriate width to optimize the SNR. If a residual baseline is present, a polynomial of order 3 or less is fitted to the spectral points where the line is not present and subtracted from the spectrum. Gaussian components were fitted to each spectral feature to obtain the line parameters.

2.6 Calibration of the Spectra

All the observed spectra were measured with the one-bit autocorrelation spectrometer. Because of this quantization, the spectrometer produces a "normalized" spectrum (Weinreb 1963). The normalization is with respect to the autocorrelation value at zero lag, which corresponds to the total power in the observed frequency band. Thus the observed on-source spectrum can be written as

$$P_{on}(\nu) = \frac{[P(\nu) + P_L\Phi(\nu - \nu_0)]G(\nu)}{\int[P(\nu) + P_L\Phi(\nu - \nu_0)]G(\nu)d\nu} \tag{2.1}$$

If we assume that the recombination line is much weaker than the continuum then

$$P_{on}(\nu) \approx \frac{[P(\nu) + P_L\Phi(\nu - \nu_0)]G(\nu)}{\int P(\nu)G(\nu)d\nu} \tag{2.2}$$

Similarly, the reference spectrum, which in our observations is obtained by switching the LO frequency (see Section 2.4), is given by

$$P_{off}(\nu) = \frac{P(\nu)G(\nu)}{\int P(\nu)G(\nu)d\nu}. \tag{2.3}$$

Here $P(\nu)$ is the power spectrum of the total system noise (i.e. receiver noise plus the continuum emission from the sky), P_L is the peak line amplitude, $\Phi(\nu)$ is the line profile function, ν_0 is the center frequency of the line and $G(\nu)$ is the overall gain function of the observing system. We assume that the gain function $G(\nu)$ is same for both reference and on-source measurements. The difference spectrum is obtained as

$$P_{diff}(\nu) = \frac{P_{on}(\nu) - P_{off}(\nu)}{P_{off}(\nu)} = \frac{P_L\Phi(\nu - \nu_0)}{P(\nu)}. \tag{2.4}$$

$P(\nu)$ is proportional to on-source system temperature. Defining the peak line antenna temperature by P_L/k, k being the Boltzmann constant, the spectrum can be calibrated in units of antenna temperature by multiplying the difference spectrum by the on-source system temperature. The on-source system temperature is obtained along with continuum measurements towards the observed positions (see Section 2.7).

Since the observed spectra are effectively convolved with the spectral resolution function, the measured difference spectrum is given by

$$P_{diff}(\nu) = \frac{[P_L\Phi(\nu - \nu_0)G(\nu)] \otimes R(\nu)}{[P(\nu)G(\nu)] \otimes R(\nu)}, \tag{2.5}$$

where $R(\nu)$ is the response function of the spectrometer. In this method of calibration, it is assumed that the width of the response function is much smaller than that of the profile function.

2.7 Continuum Measurement towards the Observed Positions

Since the objects of interest here are extended, the continuum is measured in units of antenna temperature rather than flux density. These measurements along with line antenna temperature are needed for modeling the RRL emitting region (see Chapter 5). The on-source system temperature is also obtained along with continuum measurement, which is used to calibrate the spectrum as discussed above. In few of the positions observed in Mode A, where we do not have a direct continuum measurement, the value of continuum antenna temperature (T_{CA}) is obtained from the 408 MHz all sky continuum map (Haslam et al. 1982). The method used to obtain T_{CA} from the map is also discussed here.

The antenna temperature due to a source, when observed with the ORT, and the on-source system temperature ($T_{sys,on}$) cannot be measured directly since the receiver system does not have a Cal-noise injection facility. An indirect method to determine these quantities is as follows. The increase in the antenna output power when the telescope is moved from an off-source position to an on-source position can be measured using a calibrated power meter. Thus $T_{sys,on}$ and T_{CA} can be written in terms of the off-source power or off-source system temperature $T_{sys,off}$ as

$$T_{sys,on} = a\, T_{sys,off}, \tag{2.6}$$

$$T_{CA} = (a-1)\, T_{sys,off}, \tag{2.7}$$

where a is the factor by which antenna output power is increased with respect to the off-source position. $T_{sys,off}$ consists of contribution from the sky, the receiver and the ground spillover. The contribution from the receiver plus the ground contribution is estimated to be $\sim$ 100 K (Roshi 1995). It is reasonable to assume that the contribution due to spillover is independent of the telescope position and the receiver temperature is independent of the phasing of the dipole array. The sky temperature at the off-source position is obtained as follows. The 408 MHz all-sky map of Haslam et al. (1982) was convolved by a Gaussian beam of FWHM 2.3° × 2.3°, which is approximately the FWHM of the telescope beam. The sky temperature is then scaled to 327 MHz using a spectral index of -2.7. The system temperature at the off-source position is then obtained by adding 100 K to the estimated value. $T_{sys,on}$ and T_{CA} can be obtained using the estimated $T_{sys,off}$ by applying Eq. 2.6 and Eq. 2.7.

Estimation of $T_{sys,on}$ and T_{CA} is affected by errors in measurement of the increase in on-source temperature with respect to an off-source position (i.e. the factor a) and the estimation of the off-source system temperature. To minimize the error in determining

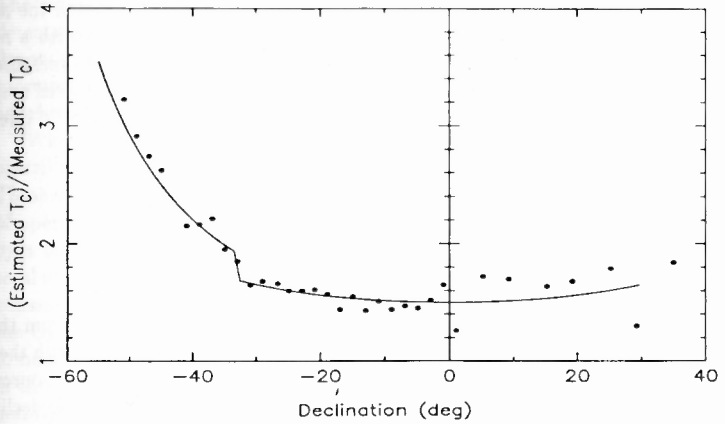

Figure 2.6: The ratio of the continuum antenna temperature obtained from the 408 MHz map to that measured using a module of the ORT is plotted as a function of declination (δ) of the source. The solid line is a function of the form $y(\delta) = 0.5 + \frac{1}{\cos(\delta)}$ for $\delta > -33^o$ and $y(\delta) = 0.5 + \frac{1}{\cos^2(\delta)}$ for $\delta < -33^o$.

the factor a an off-source position is chosen by moving the ORT in hour angle without changing the phasing and delays across the dipole array. This is because the gain of the front-end receiver system changes when the phasing of the array is changed. Another factor that can affect the measurement of a is the dynamic range of the receiver system, since in the galactic plane the sky background temperature is high and the system temperature increases by a factor of 5 – 10 when the antenna is pointed to the galactic plane. To minimize the measurement error of the factor a, the receiver system should be linear when the system temperature changes by this factor. The measured dynamic range of the front-end receiver system is about 28 dB with a bandwidth of 20 MHz. However, the dynamic range degrades in subsequent stages of the receiver system, resulting in a overall dynamic range of $\sim$ 10 dB for the receiver system when measured at the input of the recombination line receiver (i.e. at I/P1 to I/P4 in Fig. 2.4). We therefore made all the continuum measurements at an earlier stage in the receiver system where the dynamic range is $>$ 20 dB.

The estimated off-source system temperature depends on the value of the off-source sky temperature determined from the 408 MHz map. The sky temperature obtained from the 408 MHz map is a function of the beam used for convolving the map. However, we found that at the off-source position the value estimated depends only weakly on the convolving beam. We convolved the map with Gaussian beam of width ranging from $2^\circ.2 \times 2^\circ.2$ to $2^\circ.6 \times 2^\circ.6$. The change in the sky temperature at the off-source positions is typically less than 6 %.

For some of the positions for which we were unable to obtain a measurement of

the continuum antenna temperature, we estimated the values from the 408 MHz map after convolving the map with the observed beam. Since the beam shape is not known to a good accuracy and also since it is a function of the declination (the functional dependence for declinations beyond $\pm$ 35° is not known) we estimated the antenna temperature in the following way. The 408 MHz map was convolved with a nominal beam of 2°.6 × 2°.6. The antenna temperature at the positions where measurements were made was then compared with the values estimated from the convolved map. The ratio is plotted as a function of declination as shown in Fig. 2.6. The solid line shows a fit to the data points given by

$$y(\delta) = 0.5 + \frac{1}{\cos(\delta)} \text{ for } \delta > -33^o \tag{2.8}$$

$$= 0.5 + \frac{1}{\cos^2(\delta)} \text{ for } \delta < -33^o \tag{2.9}$$

This plot gives the factor by which the antenna temperature estimated from the convolved 408 MHz map is to be multiplied to obtain the value as measured with the ORT. The plot also gives the dependence of this factor on the declination of the source. The plot clearly shows that the beam of the ORT has a $\cos^2(\delta)$ dependence on declination for $\delta < -35°$. This is because the primary pattern of the feed itself has approximately a $\cos(\delta)$ dependence for $\delta > |35^o|$.

2.7.1 Beam Efficiency of a Module of the ORT

The method described above can also be used to measure the main beam efficiency (η_B) of a single module of the ORT. The beam efficiency is defined as $\eta_B \equiv \frac{\Omega_B}{\int_{4\pi} B(\Omega) \mathrm{d}\Omega}$, where $B(\Omega)$ is the response of the telescope and Ω_B is the half power beam width. η_B is required to estimate the line and continuum brightness temperature from the respective measured antenna temperatures (see Eq. 2.13; also see Chapter 5). We observed the sources Hydra A (RA (1950): $09^h15^m41^s$, DEC (1950): $-11°53'08''$) and Crab (RA (1950): $05^h31^m31^s$, DEC (1950): $+21°58'54''$) using the module N3 and measured the antenna temperature as described above. The off-source position for Hydra A was chosen as RA(1950) $02^h15^m00^s$ and declination same as that of Hydra A. After correcting for the difference in the sky background between the off-source position and near Hydra A, the measured antenna temperature due to Hydra A is 20.7 K. Taking the flux density of Hydra A at 327 MHz as 166.2 Jy and correcting for projection effects, we get 0.13 K/Jy (at $\delta = 0°$) as the antenna temperature per flux density. Since the FWHM of the beam at $\delta = 0°$, is 2°.3 (in RA) × 2°.2 (in DEC), the implied beam efficiency is 64 %.

We repeated the above measurements on Crab nebula. The off-source position was chosen at RA(1950) $03^h30^m00^s$ with the declination same as that of Crab. The off-source sky temperature obtained from the 408 MHz map is 50 K. The measured antenna temperature due to Crab is 159 K. Taking the flux density of Crab nebula at 327 MHz as 1320 Jy, we again get 0.13 K/Jy (at $\delta = 0°$) and the implied beam efficiency is 65 %.

2.8 Sensitivity of the Observations

The sensitivity of the observations is a measure of the weakest spectral line that is detectable with a given frequency resolution and integration time. The sensitivity depends on various factors such as the receiver temperature, antenna temperature due to source and method used for measuring the spectra. A brief discussion of these factors as relevant for the present observation is given below.

When the telescope is pointed at a source of interest, the output signal includes contributions from the receiver, sky background and ground pickup due to spillover. These signals usually have a spectral density which is uniform over the total bandwidth of operation of the telescope. Hence they can be characterized (in the radio regime) by a temperature at which a resistor produces the same amount of white noise. The total system temperature is the sum of the antenna temperature due to the background emission (see below) and the contribution from the receiver and ground pickup. For the ORT, the total contribution from the receiver and the ground has been estimated to be about 100 K (Roshi 1995). The observations presented in this thesis were made in the galactic plane and hence sky background emission is dominated by the galactic non-thermal emission.

The antenna temperature (T_A) due to a source is related to its brightness temperature (T_B) with the following relations (Christiansen & Högbom 1985)

$$\frac{1}{2}SA_{eff} = KT_A, \tag{2.10}$$

$$S = \frac{2kT_B\Omega_s}{\lambda^2}, \tag{2.11}$$

$$A_{eff} = \frac{\lambda^2}{\int_{4\pi} B(\Omega)\mathrm{d}\Omega}, \tag{2.12}$$

$$T_A = T_B\frac{\Omega_s}{\int_{4\pi} B(\Omega)\mathrm{d}\Omega} = T_B\frac{\Omega_s\eta_B}{\Omega_B}. \tag{2.13}$$

Here S is the flux density of the source, k is the Boltzmann constant, A_{eff} is the effective area of the telescope, λ is the observing wavelength, Ω_s is the source solid angle, $B(\Omega)$ is the response of the telescope, Ω_B is the half power beam width and η_B is the beam efficiency factor. If the source is omnipresent (e.g. the sky background), then in Equations 2.11 & 2.13 the source solid angle should be replaced by the telescope beam and therefore $T_A = T_B$. A more practical situation where $T_A \approx T_B$ arises when the angular extent of the source is much larger than Ω_B. Equation 2.12 implies that under such a situation there is no increase in sensitivity when the collecting area of the telescope is increased. Observations in Mode A described in Section 2.4.1 corresponds to this situation. From previous observations (e.g. Lockman 1976), it is known that low frequency RRL emission regions in the galactic plane are very extended. Thus the large scale properties of the regions can be studied in Mode A (beam size $\sim 2^\circ \times 2^\circ$) without any significant loss of sensitivity. However, in reality, the RRL emission region may be patchy with many patches within the $2^\circ \times 2^\circ$ beam. Observations in Mode B (beam size $2^\circ \times 6'$) are likely to reveal any such patchiness.

The sensitivity also depends on the method used for spectral measurement. In these observations, the spectrum is measured using a digital autocorrelator. The finite-bit sampling of the data required for the digital system adds noise, called quantization noise. The magnitude of this noise depends on the number of bits used for quantization. We

have used one bit quantization and sampled the data at Nyquist rate. The noise in the spectrum is increased, in this case, by a factor of $\frac{\pi}{2}$ (Weinreb 1963) compared to sampling with infinite number of bits (or analog system).

In these observations, the sensitivity is further improved by averaging several spectra which are measured simultaneously. In Mode A, two of the ORT modules are pointed in the same directions and each module measures four RRL transitions simultaneously. It is clear that the SNR is improved by a factor of 2 by averaging the 4 RRL transitions. However, any improvement in the SNR by averaging the spectra from the two modules depends on whether the noise fluctuations are independent. The fluctuations due to the receiver noise will obviously be uncorrelated between any two modules since the receiver systems are independent. The signals received from the sky, however, have a common origin. Will the noise in the spectra from the two modules be correlated due to this ? As described earlier, the non-thermal background dominates over the receiver noise in most of the positions in the galactic plane that have been observed. The fluctuations at the output of the two modules due to sky-background become independent if the sky background is "resolved" by an interferometer with a baseline equal to the separation between the two modules. In other words, if the sky background is uniform over an angle $\theta > \frac{\lambda}{D}$ where D is the physical separation between the modules projected in the direction of the source, then the output fluctuations are independent. In our observations we have selected modules which are physically separated by ~ 300 m. Thus if the galactic background emission is uniform over $\sim 12'$, then there will not be any correlated noise in the spectra measured simultaneously with the 2 modules. Thus an improvement in the SNR of $\sqrt{2}$ can be expected by averaging spectra from two modules measured simultaneously.

In Mode B, the two beams are pointed at different directions in the sky. Hence there are no signals of common origin that are received by the telescope from the sky (except the side lobe of one beam pointing in the same direction as the main or side lobe of the other; we neglect this effect here). However, the receiver noise have a common origin since the two beams are produced by adding signals from the same 22 modules but with different phase gradients. The problem of correlated noise between different beams of the ORT has been discussed in detail by Singal (1985). He has shown that the noise correlation in different beam has a functional dependence similar to the beam shape itself, which implies that the correlation goes to zero at the null of the telescope response. We have therefore selected two beams whose main lobes are separated by $\sim 5'.5$, which is the expected position of the null from the beam center.

The RMS noise in the difference spectrum after integrating for τ hours is given by

$$\Delta T = \frac{\pi}{2}\sqrt{\frac{2}{\Delta\nu\tau}}0.866T_{sys}. \tag{2.14}$$

Here ΔT is the RMS noise in K, T_{sys} is the system temperature, $\Delta\nu$ is the frequency resolution in Hz and τ is in sec. The factor $\frac{\pi}{2}$ is due to the one-bit quantization, 0.866 is due to cosine weighting of the autocorrelation function and the factor $\sqrt{2}$ arises because the bandpass correction is made by dividing by the reference spectra. Typical integration time for each position is ~ 3 hrs. Taking $T_{sys} = 300$ K, which is a typical value, and $\Delta\nu = 5$ kHz the RMS noise achieved is ~ 80 mK. By averaging the eight spectra the RMS noise reduces to ~ 30 mK.

2.9 Summary

In this chapter, I have described the equipment used for the observations, the procedures of observation and data reduction, the calibration of the observed spectrum and finally the sensitivity of the observations. The Ooty Radio Telescope and the multi-line spectrometer used for the observations are described. The observations presented in this thesis are made with two different angular resolutions – (a) $2^\circ \times 2^\circ$ (low resolution mode) and (b) $2^\circ \times 6'$ (high resolution mode). Details of these observing modes, and continuum antenna temperature measurements are also presented in this chapter.